

Optical Performance of Commercial Liquid Lens Assemblies in Microgravity

Shreeyam Kacker^{a,*}, Kerri L. Cahoy^a

^aMassachusetts Institute of Technology, Space Telecommunications, Astronomy and Radiation Laboratory, Department of Aeronautics and Astronautics, Cambridge, MA 02139, United States

Abstract. Liquid lenses have been utilized in various applications due to their low size, weight, power, and cost. They have potential for use in space applications such as focus compensation, optical communications, and imaging systems. However, liquid lenses have not yet been evaluated for us in space environment. This work focuses on characterizing operational differences of commercially available liquid lenses from Corning Varioptic and Optotune between Earth gravity, microgravity, and hypergravity environments. Results show a linear drift in tip/tilt of 0.79 mrad and 4.13 mrad going from 1 g to 0 g for the Corning Varioptic A-39N0 lens and Optotune EL-16-40-TC-VIS lenses respectively, with lower optical aberrations in microgravity. Additionally, focusing power increases going from 1 g to 0 g by 0.059 D for the Corning Varioptic lenses and 0.039 D for the Optotune lenses. This work is part of a wider space environment study showing that Corning Varioptic and Optotune’s commercial liquid lenses withstand thermal vacuum, typical low Earth orbit ionizing radiation exposure, and effectively handle high-intensity laser power in a vacuum without significant damage.

Keywords: Liquid lens, space optics, microgravity, beam steering, optical communications, small satellites.

*Shreeyam Kacker, E-mail: shreeyam@mit.edu

1 Introduction

Liquid lenses are compact, nonmechanical focus-tunable lenses that use a liquid to change their focal length. Due to their low size, weight, power, and cost (SWaP-C) they are attractive for space applications, where they could be used for focus compensation, optical communications, and more. However, liquid lenses, have not been fully evaluated for use in the space environment. Previous work has subjected liquid lenses to thermal vacuum (TVAC) testing,^{1,2} but other space environment tests such as ionizing radiation and microgravity has not yet been conducted. This work presents results using commercially available liquid lenses from Corning Varioptic and Optotune on a microgravity flight to characterize differences in operation between Earth gravity and microgravity. Microgravity testing is especially important, as the optical fluid sags in gravity causing increased wavefront error and aberrations.³

This work is part of development for the Miniature Optical Steered Antenna for Inter-satellite Communication (MOSAIC) project

which aims to utilize liquid lenses for a hemispherically steering lasercom terminal for small satellites, for which reliable operation in the space environment required.^{1,2,4,5} The MO-SAIC project aims to utilize liquid lens arrays for beam steering and laser communication on small satellites. The project seeks to construct a compact, nonmechanical lasercom transceiver with integrated beam steering for small satellites using liquid lenses. The transceiver design is based on a previous design by Zohrabi⁶ utilizing a single on-axis lens for divergence control and an additional two lenses offset in x and y for 2D steering, initially proposed for LIDAR. Additionally, this work is part of a broader space environment evaluation effort including ionizing radiation testing and vacuum power handling performance, for which more details can be found in the full study by Kacker⁵ – in summary, commercial liquid lenses from Corning Varioptic and Optotune perform well during TVAC testing, do not show gross discoloration when exposed to ionizing radiation equivalent to 10 years of low

49 Earth orbit, and can handle many over 2 W of
 50 laser power in vacuum without damage

51 Additionally, this work is part of a broader
 52 space environment evaluation for which more
 53 details can be found in the full study.⁵ In sum-
 54 mmary, the commercial liquid lenses tested in
 55 this work also survive and operate in (TVAC),
 56 have no significant discoloration under typical
 57 space mission exposure to ionizing radiation
 58 and can handle multiple watts of laser power
 59 in vacuum.

60 2 Background

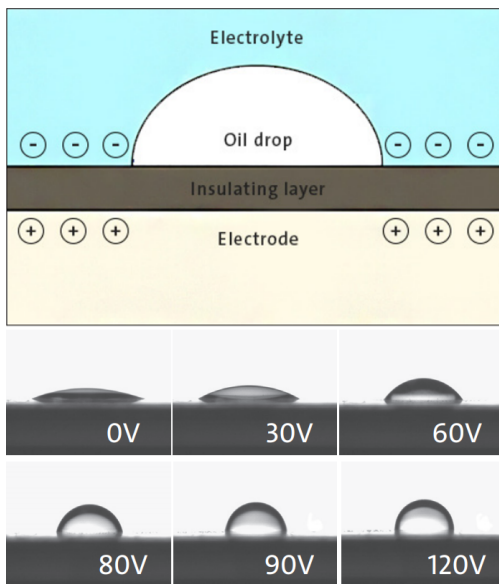


Fig 1: Diagram showing electrowetting principle of operation for Corning Varioptic lenses.⁷

61 Liquid lenses have applications in machine
 62 vision,^{3,7} phone cameras,⁸ microscopy,⁹ opti-
 63 cal communications¹⁰⁻¹⁴ and more due to their
 64 compactness and depending on the lens tech-
 65 nology, low power. Optotune and Corning Vari-
 66 optic are the two main companies making liq-
 67 uid lenses, each producing lenses with differ-
 68 ent operating principles. Corning Varioptic's
 69 liquid lenses employ electrowetting technol-
 70 ogy, where an applied electric field causes an
 71 oil droplet's contact angle with an insulator

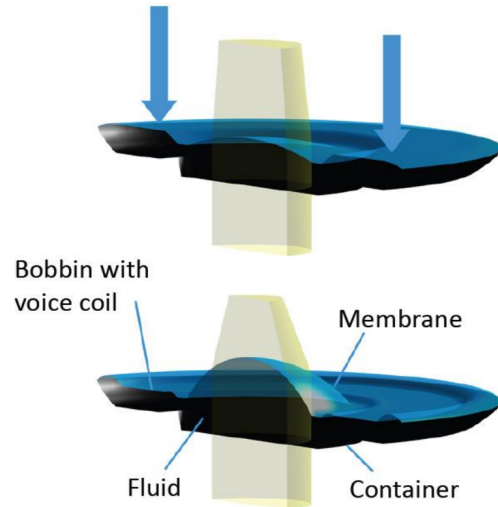


Fig 2: Diagram showing pressure based principle of operation for Optotune lenses.³

72 to change,⁷ whereas Optotune's lenses func-
 73 tion based on pressure, with a voice coil caus-
 74 ing fluid to displace into the center of a mem-
 75 brane.³ Diagrams of how Corning Varioptic's
 76 and Optotune's lenses work are shown in Fig. 1
 77 and Fig. 2 respectively.

78 For a satellite lasercom terminals, evaluat-
 79 ing liquid lens performance in the space envi-
 80 ronment is important, including zero gravity
 81 testing. Previous work has shown that liquid
 82 lenses can survive and operate in other space
 83 environment conditions, including thermal vac-
 84 uum testing^{1,2} However, because liquid lenses
 85 use liquids to be focus tune-able, they experi-
 86 ence a higher wavefront error and aberrations
 87 in the presence of gravity, with the Optotune
 88 lenses used in this study having an increased
 89 wavefront error of 50 nm³ in Earth gravity con-
 90 ditions, measured by placing the lens in dif-
 91 ferent orientations. Characterizing liquid lens
 92 performance under zero gravity conditions is
 93 crucial for space applications.

94 Previous work on evaluating the effects of
 95 gravity on liquid lenses has been conducted
 96 by changing the lens orientation, but this tech-
 97 nique cannot eliminate the effects of gravity
 98 entirely.¹⁵ This work presents zero gravity data
 99 from parabolic aircraft testing in order to un-

100 understand the effects on optical performance.

101 3 Approach

102 3.1 Experimental Setup

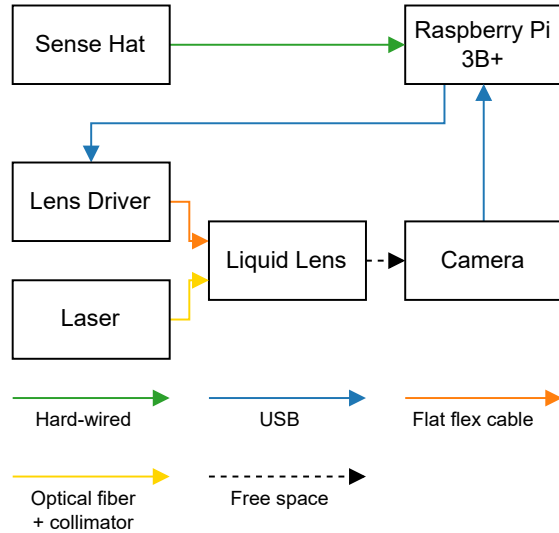


Fig 3: Block diagram of experiment components.

103 The experiment consists of two independent
 104 optical trains, each operated by a dedi-
 105 cated Raspberry Pi. One optical train is for the
 106 Corning Varioptic lens, while the other is dedi-
 107 cated for the Optotune lens. A block diagram
 108 of one of these optical trains is shown in Fig. 3,
 109 and a diagram of the optical components is
 110 shown in Fig. 4, with further details about the
 111 hardware used in the experiment given in Ta-
 112 ble 1. A photograph of the experiment on the
 113 aircraft is also shown in Fig. 6.

114 During operation, lens commands are swept
 115 through and the resulting spot on a detector is
 116 imaged. Measurements are taken for 64 lens
 117 commands surrounding the focus, from 49.5 V
 118 to 53.5 V for the Corning Varioptic lens and
 119 70 mA to 110 mA for the Optotune lens. The
 120 fastest data capture rate of every 300 ms and
 121 the 15-25 second parabola duration guide this
 122 quantity, with 64 points being approximately
 123 the number of points that can be captured in a
 124 single parabola, giving a complete sweep. The

125 measured quantities include the image, accel-
 126 eration (3-axis), gyro (3-axis), magnetometer
 127 (3-axis), and temperature. A flowchart of the
 128 software is shown in Fig. 5.

129 3.2 Spot Analysis

130 Using the data, the imaged spots on the detec-
 131 tor can be analyzed to understand operational
 132 differences between the gravity regimes. As
 133 the beams deform significantly between grav-
 134 ity regimes, fitting standard Gaussian beams to
 135 understand how beam width varies is difficult.
 136 Instead, a metric for the relative spot width
 137 is used as shown in Equation 1, which is the
 138 square root of the number of pixels above an
 139 intensity threshold, can be used as a proxy for
 140 beam diameter. The limitations of this metric
 141 are that while it cannot be used for absolute
 142 beam width measurements, it can be used to
 143 understand relative changes.

144 With the threshold set to just above the
 145 noise floor of the sensor, this measurement
 146 should vary hyperbolically, in the same way
 147 that absolute beam diameter would.

$$r_{\text{spot}} = \sqrt{n. \text{ pixels above threshold}} \quad (1)$$

148 4 Results and Discussion

149 In this section, measurements from the flight
 150 are used to understand how lens performance
 151 changes between zero gravity, Earth gravity,
 152 and hypergravity conditions. The spot analysis
 153 approach is used to understand how the lenses
 154 change in focal length and centroiding is used
 155 to determine how the point spread functions
 156 (PSFs) change in location for each condition.

157 4.1 Flight Profile and Measurements

158 The flight profile of the experiment is shown
 159 in Fig. 7. The profile shows all 20 parabolas,
 160 including the two parabolas each in Lunar
 161 and Martian gravity. The takeoff and landing
 162 phases are also clearly visible. Fig. 8 shows

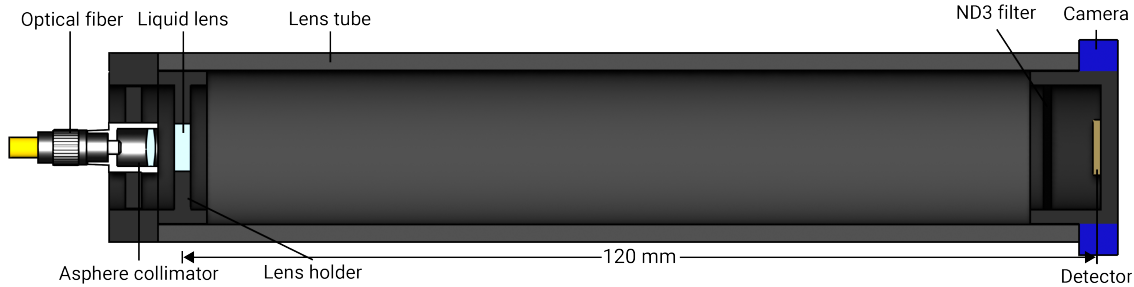


Fig 4: Diagram of single optical train in experimental setup.

Table 1: List of hardware used in experiment.

Device	Property	Value
Liquid Lens	Model (Corning Varioptic)	A-39N0
	Model (Optotune)	EL-16-40-TC-VIS-20D
Laser	Type	1 mW Fiber Tester
	Wavelength	633 nm
Collimator	Model	Thorlabs F220FC-B
	Wavelength	633 nm
	$1/e^2$ Diameter	2.1 mm
Camera	Make	Matrix Vision
	Model	mvBlueFox-IGC 205v
	Pixel Pitch	$2.2 \mu\text{m}$
	Binning	2×2
	Resolution	2592×1944
Raspberry Pi	Bit depth	10 bit
	Model	3B+
	Hat	Sense Hat

163 a zoomed in view of the second set of five
164 parabolas.

165 Measurements of hypergravity experienced
166 during the ascent phases of each parabola are
167 also recorded, providing additional data for
168 comparison. A histogram of the recorded g-
169 force for all samples is shown in Table 9. Ap-
170 proximately 20,000 samples were collected for
171 both Corning Varioptic and Optotune lenses.

172 4.2 Spot Analysis

173 Fig. 10 and Fig. 11 show individual focused
174 samples from each gravity regime for the Corn-
175 ing Varioptic and Optotune lenses, respectively.

176 As a first comparison, the Corning Varioptic
177 focused spots have much smaller increases in
178 tip/tilt and coma compared to the Optotune
179 ones. The Optotune samples show very pro-
180 nounced coma and deformation in higher grav-
181 ity regimes. Some minor reflections are also
182 visible for both Corning Varioptic and Opto-
183 tune samples, although much more visible for
184 the former than the latter.

185 The results for relative spot width over var-
186 ious lens commands are shown in Fig. 12 and
187 Fig. 13. Overall, the analysis shows consistent
188 results for both microgravity and Earth gravity
189 with a few key differences. Both lenses show

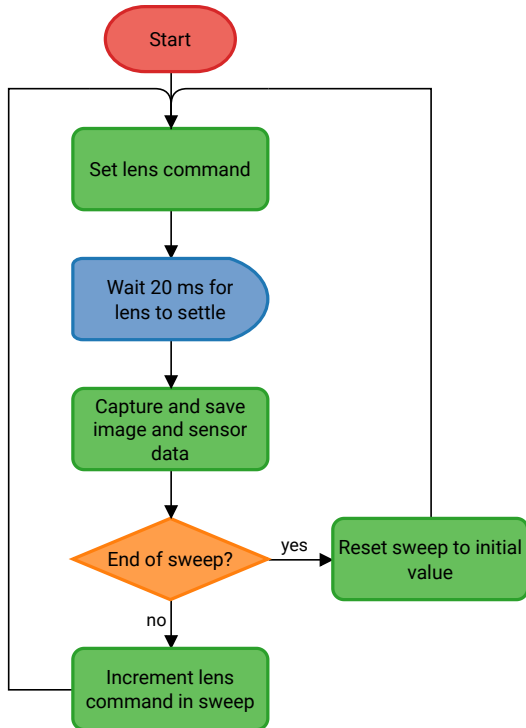


Fig 5: Flowchart of experiment flight software that runs continuously and records samples.

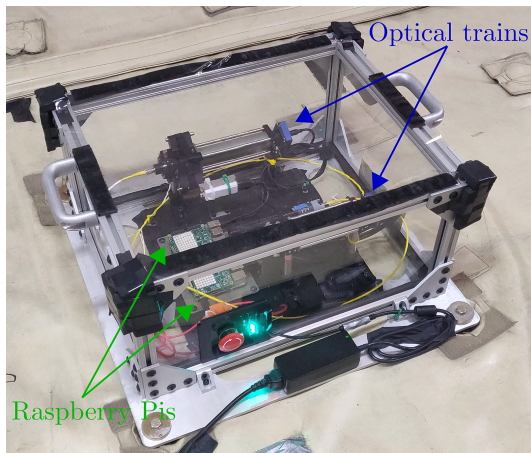


Fig 6: Experimental setup affixed to the floor of the zero gravity aircraft.

190 marginally increased focal length for the same
 191 lens command, and slightly lower relative spot
 192 width around the focal point. The increased
 193 focal length could be due to gravity providing
 194 some resistance to the actuation force that gets
 195 transferred horizontally due to surface tension
 196 on the lenses, whereas the smaller relative spot
 197 width is most likely due to lower aberrations in

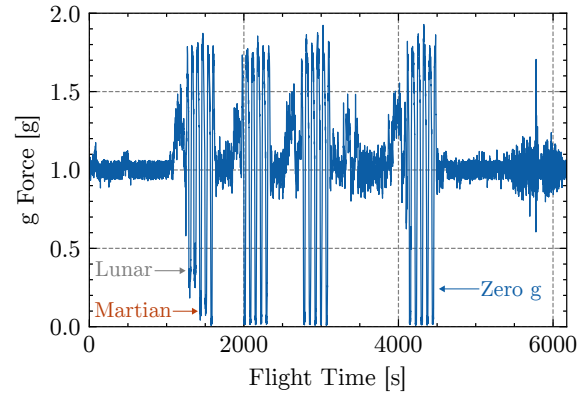


Fig 7: Complete parabolic flight profile of g-force against time showing takeoff, landing, and full 20 parabolas.

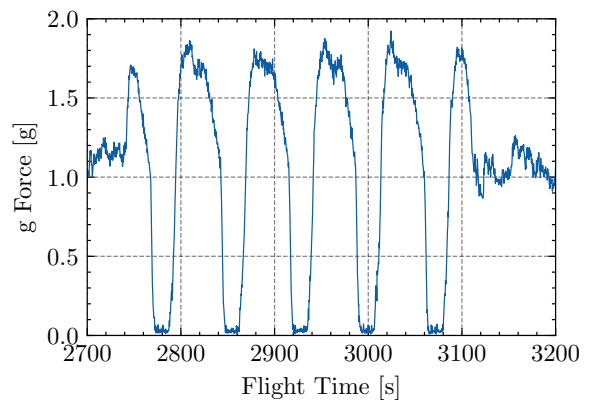


Fig 8: Zoomed view of g-force magnitude over time for second set of five parabolas. All parabolas in this set are zero gravity parabolas.

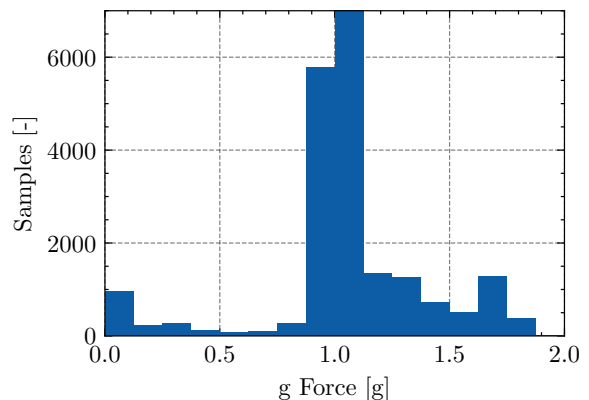


Fig 9: Histogram of total samples with g-force of each sample.

198 microgravity causing less smearing of the lens
 199 command. Lens focusing power increased in

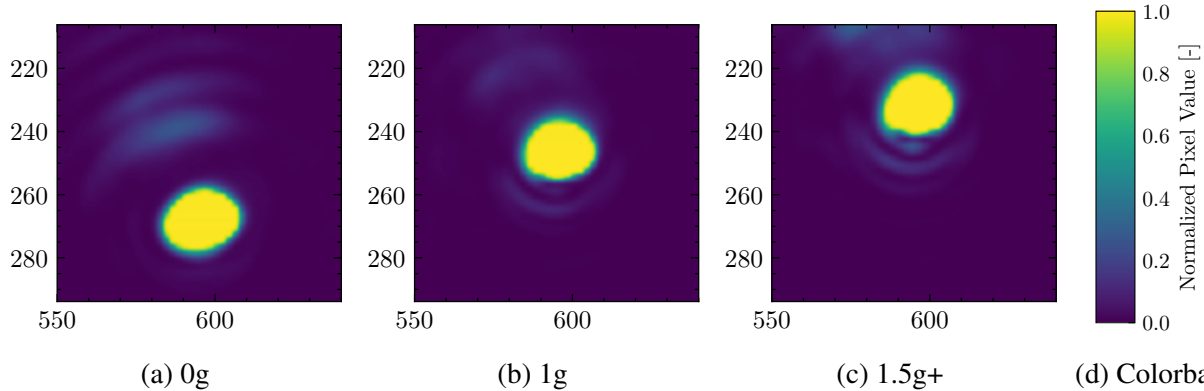


Fig 10: Normalized images of focused individual Corning Varioptic samples from each gravity regime. Increasing gravity shows minor increases in tip/tilt and coma.

microgravity by 0.059 D for the Corning Varioptic A-39N0 and 0.039 D for the Optotune EL-16-40-TC-VIS lenses.

The Optotune lenses have well-constrained and consistent error bars throughout the lens commands, but the Corning Varioptic lenses show much larger error bars across the extremes of the sweep. This increased error caused the hyperbolic fits to be constrained towards the central section of points. The deviation seems due to variation in the samples causing parts of the image to pass below the threshold for relative spot width. Examples of samples at the same lens command but with different relative spot widths are shown in Fig. 14 and Fig. 15. An interesting defocus pattern from the Corning Varioptic lens forms, which then appears to be smeared, causing the high value for relative spot width in Fig. 14. The cause of this smearing is not obvious, but could be due to vibration of the liquid lens during the flight. There is no significant correlation of this smearing to particular times of the flight or parabola. Some of the vibration also appears to make its way into the image as a result of circular standing waves, visible in the center of both Fig. 14 and Fig. 15.

4.3 Centroid Analysis

Fig. 16 and Fig. 17 show stacked and averaged images of the spot on the detector taken

at each of their focal commands. The dominant aberration present is tip/tilt, with large changes between each gravity regime as summarized in Table 2 and measured using centroiding the PSFs from each lens. The change in tip/tilt is linear with the effect of gravity, with the linear regression shown in Fig. 18 and Fig. 19 for the Corning Varioptic and Optotune lenses respectively. Both sets of lenses adhere well to the linear fit, with an R^2 value of 0.78 for the Corning Varioptic lenses and 0.97 for the Optotune lenses. The R^2 value for the Corning Varioptic lenses is likely larger due to the smaller focused spot on the detector and the resulting increase in quantization noise when centroiding the PSF.

Qualitatively, it can also be seen in Fig. 10 and Fig. 11 that coma and astigmatism are also present, especially in hypergravity regimes. Corning Varioptic lenses exhibit less change in tip/tilt and maintain nearly identical optical performance. Optotune lenses show a larger change in tip/tilt, with significant coma observed in the hypergravity regime, as shown in Fig. 17.

The imaged PSFs for the Corning Varioptic lenses are well-contained, with no observable spread in hypergravity as compared to microgravity. The spots for the Optotune lenses are more spread out, suggesting that vibration or other environmental factors may have impacted the experiment and contributed to the

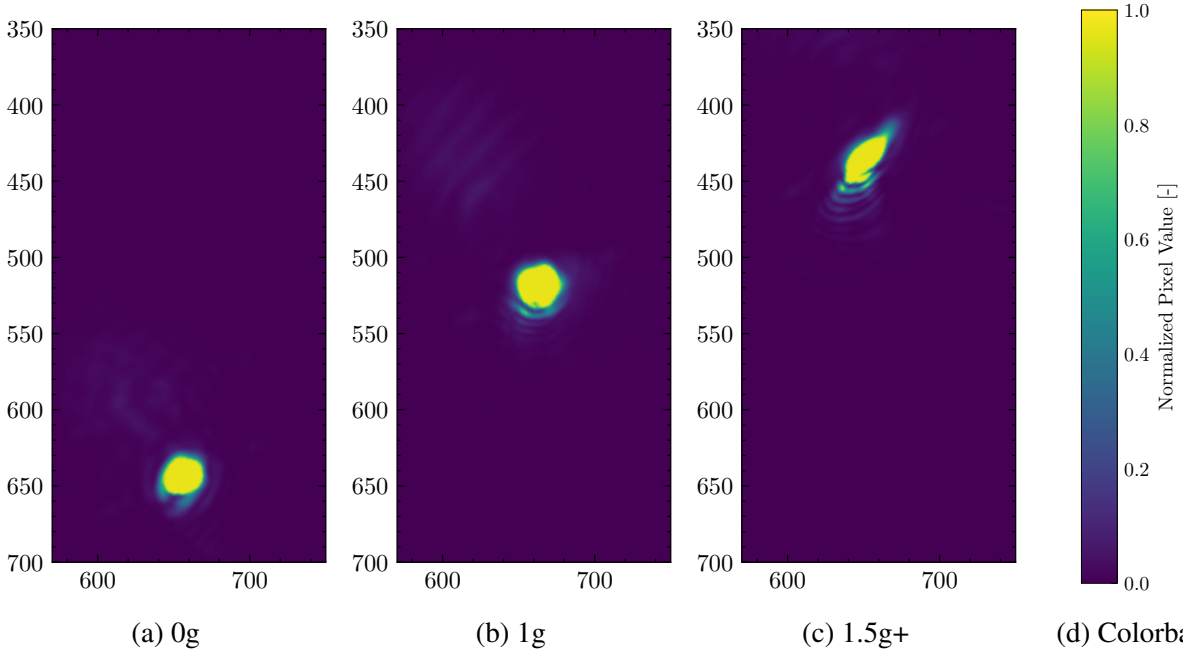


Fig 11: Normalized images of focused individual Optotune samples from each gravity regime. Increases in gravity show larger increases in tip/tilt, coma, and smearing as compared to Fig. 10.

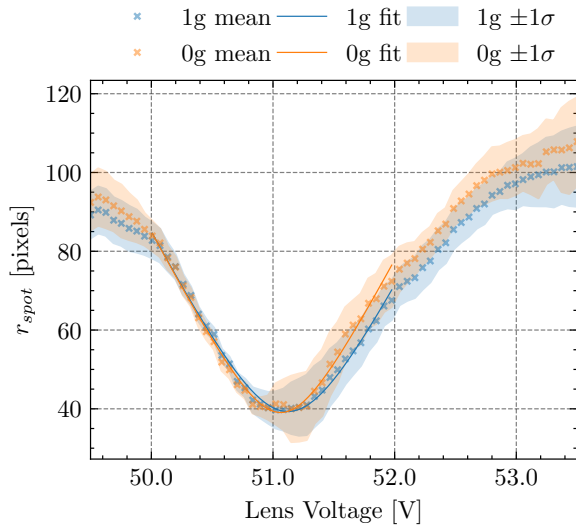


Fig 12: Relative spot width for sweep of lens commands for Corning Varioptic lenses, with associated hyperbolic fit and error bars.

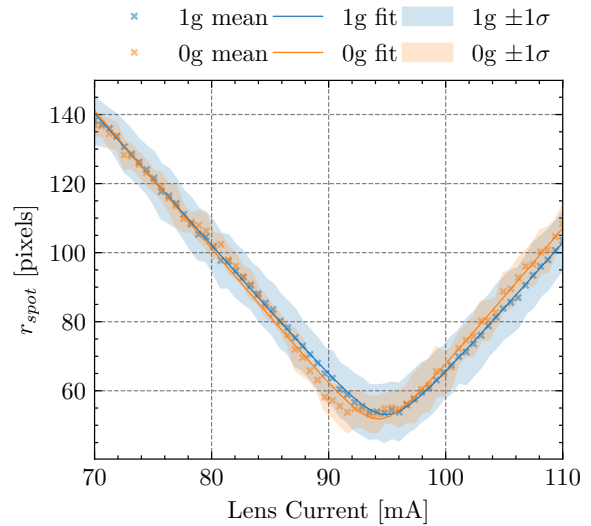


Fig 13: Relative spot width for sweep of lens commands for Optotune lenses, with associated hyperbolic fit and error bars.

261 observed aberrations. However, the imaged
 262 spots look visually tighter in microgravity, sug-
 263 gesting that there may be a gravity-dependent
 264 effect. The presence of more fluid in Optotune
 265 lenses may be a contributing factor to their
 266 optical performance being more significantly

267 affected by environmental conditions. A an ideal-
 268 ized diagram showing how fluid deformation
 269 could cause the resultant aberrations is shown
 270 in Fig. 20, although in reality, there would still
 271 be some minor fluid curvature at 0 g conditions
 272 due to surface tension.

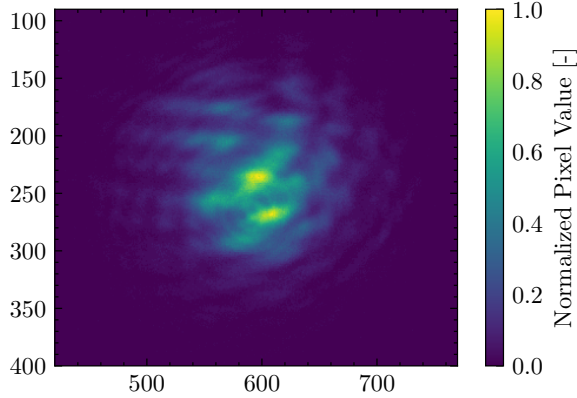


Fig 14: Example Corning Varioptic sample at 53.5 V lens voltage with high relative spot width caused by smeared features.

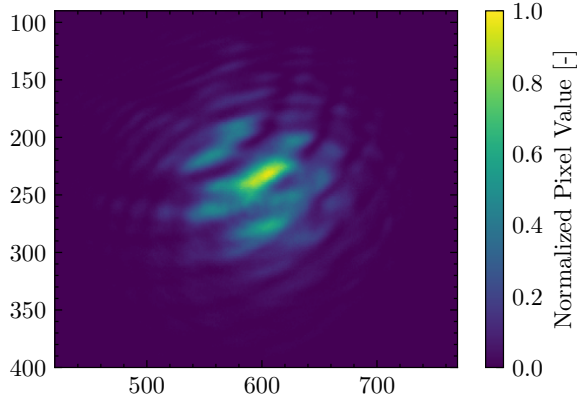


Fig 15: Example Corning Varioptic sample with low relative spot width, with identical lens command and gravity conditions as Fig. 14

273 4.4 Temperature Drift

274 Both liquid lenses used in this experiment have
 275 been shown to drift in focal length due to temper-
 276 ature variations. A temperature plot for both
 277 lenses as shown in Fig. 21 indicates that temper-
 278 ature throughout the parabolas was within
 279 4 °C for all of the parabolas, with a gradual de-
 280 crease after the lenses reached the peak temper-
 281 ature, as measured on the Raspberry Pi Sense-
 282 Hat modules. The Optotune temperature was
 283 slightly higher than the Corning temperature
 284 during the flight, which is expected as Op-
 285 totune lenses generate heat from their voice
 286 coil and high current operation. Histograms as
 287 shown in Fig. 22 and Fig. 23 reveal that a vast

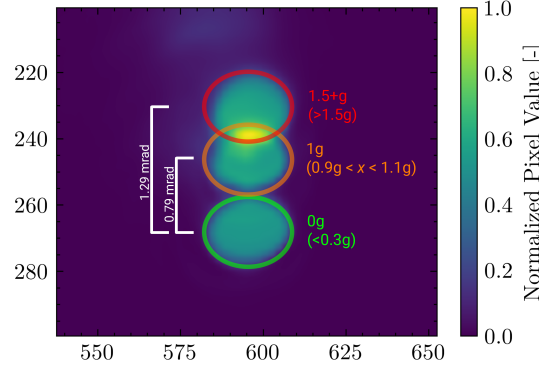


Fig 16: Image of stacked and averaged spots for each gravity environment for Corning Varioptic lenses (n: 0 g = 20, 1 g = 206, 1.5+ g = 37).

Table 2: Change in tip/tilt of centroided spots for each regime, referenced to 0 g as a baseline.

Regime	Tip/Tilt [mrad]	
	Corning Varioptic	Optotune
1 g	0.79	4.13
1.5+ g	1.29	6.31

288 majority (75%) of the 0 g and 1 g data points
 289 are in the same range, effectively controlling
 290 for temperature drift during the experiment.
 291 Moreover, hypergravity and zero gravity data
 292 are comparable since temperature histograms
 293 are almost identical, indicating that the temper-
 294 ature is adequately controlled during the exper-
 295 iment. Interestingly, microgravity parabolas
 296 can be observed in the temperature plot, per-
 297 haps due to hydrostatic forces when transition-
 298 ing into hypergravity causing redistribution of
 299 air inside the aircraft cabin.

300 5 Conclusions and Future Work

301 This work shows that liquid lenses perform
 302 well in microgravity, with reduced overall aber-
 303 rations, slight change in focusing behaviour
 304 and a change in tip/tilt. A summary of the
 305 quantitative results is shown in Table 3. A
 306 more pronounced disparity in operation is ev-
 307 ident for Optotune lenses as compared with
 308 Corning Varioptic lenses, which is likely due

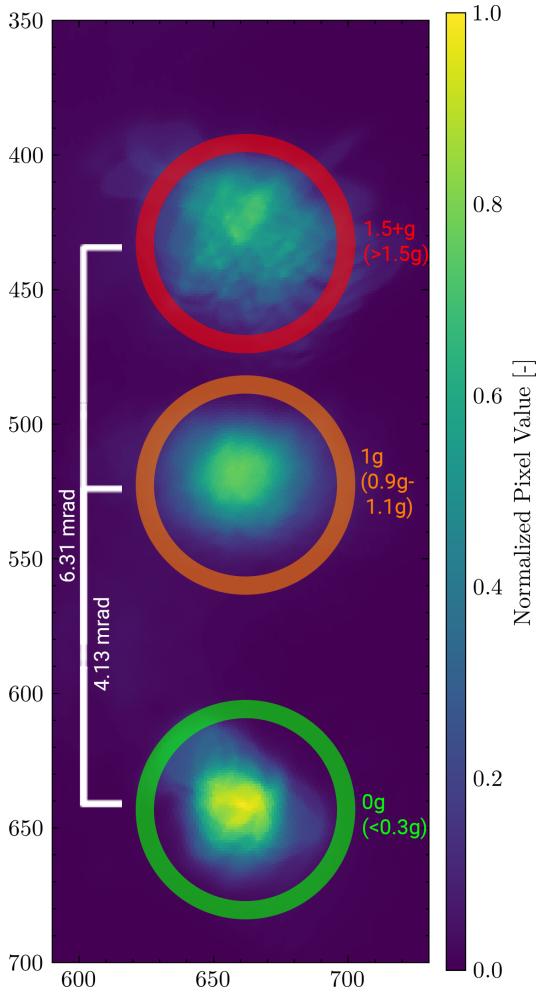


Fig 17: Image of stacked and averaged spots for each gravity environment for Optotune lenses (n: 0 g = 17, 1 g = 164, 1.5+ g = 26).

309 to their larger aperture size holding more fluid
310 volume.

311 During the microgravity flight, changes in
312 temperature were small and limited to approx-
313 imately 10 °C in the worst case. Prior studies
314 have also shown that such fluctuations do not
315 have a significant influence on the results.^{1,2}

316 In combination with previous work on space
317 environment evaluation,^{1,2,5} these results show
318 that liquid lenses are well suited for space-
319 based optical systems. Their low SWaP-C and
320 improved performance in microgravity in addi-
321 tion to previously studied operation in thermal
322 vacuum and ionizing radiation effects make
323 them a suitable option for use in a variety of

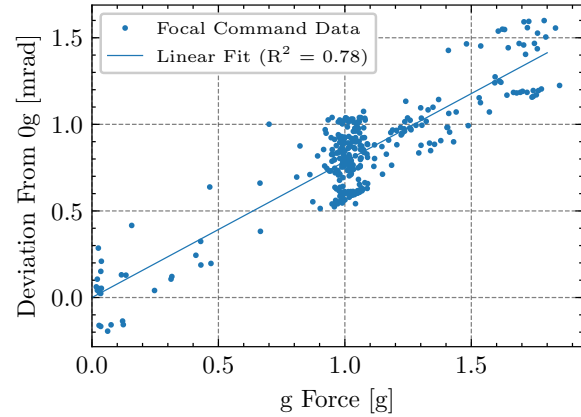


Fig 18: Linear regression of tip/tilt of focused samples against sample gravity conditions.

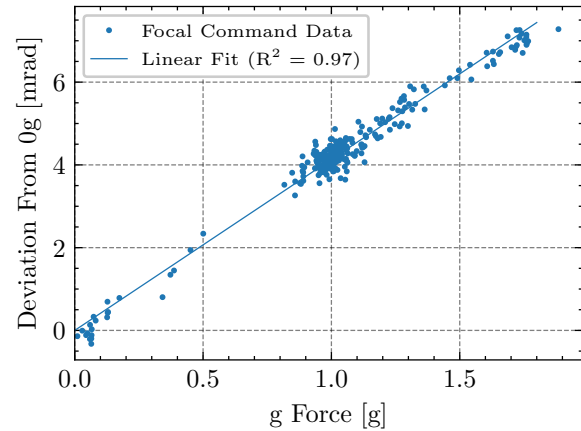


Fig 19: Linear regression of tip/tilt of focused samples against sample gravity conditions.

324 space-related applications.⁵

325 Future work includes evaluating different
326 control schemes in order to do closed-loop
327 pointing and tracking, as well as to compen-
328 sate for the change in tip/tilt in different gravity
329 conditions.

330 Further study of vibrations is needed, uti-
331 lizing a vibrometer or faster IMU readout due
332 to effects in smeared data points. With the
333 data taken in this experiment, vibration could
334 potentially be quantified using some of the re-
335 sultant standing waves observed on the sample
336 images.

337 Additionally, wavefront error is not evalu-
338 ated in this study, as a wavefront sensor was
339 not used during the microgravity flight. Evalu-

Table 3: Summary of changes in quantitatively determined properties of lenses, referenced to 0 g as a baseline.

Property	Units	Change from 0 g to 1 g	
		Corning Varioptic	Optotune
Tip/Tilt	mrad	0.79	4.13
Focal Length	Dioptres	-0.059	-0.039

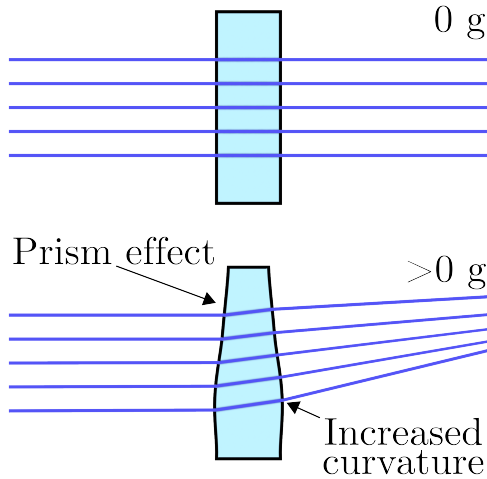


Fig 20: Potential physical mechanism explaining observed aberrations. Optical fluid sags to the bottom of the enclosure, causing slants in the side, which causes tip/tilt like a prism. Additionally, fluid curvature on the optical membrane creates higher order aberrations, such as coma and astigmatism.

340 ating the wavefront error using phase retrieval
 341 algorithms such as the Gerchberg-Saxton¹⁶
 342 algorithm, Misell’s algorithm,¹⁷ and other non-
 343 linear phase retrieval methods were attempted,
 344 but this process resulted in too much error and
 345 difficulty in convergence to obtain usable re-
 346 sults.

347 Disclosures

348 The authors declare that they have no conflicts
 349 of interest relevant to the content of this article.

350 Code, Data, and Materials Availability

351 Code and instructions for accessing data are
 352 available at this URL: <https://github.com/MIT-STARLab/mosaic-zero-g-code>.
 353

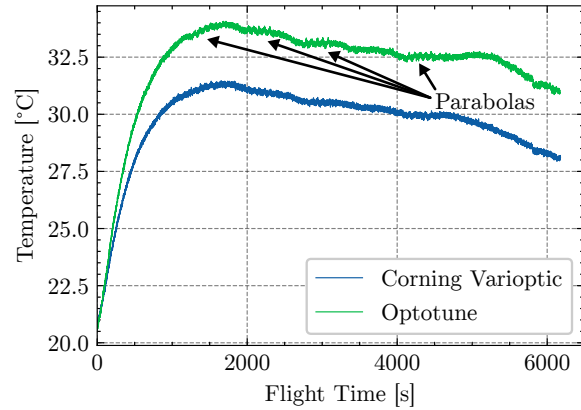


Fig 21: Temperature profile recorded on Raspberry Pi hat throughout flight. Optotune lenses due to their self heating have a higher temperature throughout the flight. Additionally, each parabola can be seen to have a very small impact on recorded temperature.

354 Acknowledgments

355 This work was supported by Early Stage Inno-
 356 vations grant 80NSSC19K0217 from NASA’s
 357 Space Technology Research Grants Program.
 358 The authors would like to thank Dr. Sarah Ted-
 359 der at NASA Glenn Research Center for her
 360 support and correspondence over the course of
 361 the program.

362 The authors would also like to thank Ariel
 363 Ekblaw, Sean Auffinger, and the rest of the
 364 MIT Media Lab Space Exploration Initiative
 365 for their support in organizing the zero gravity
 366 flight. Additionally, the authors appreciate the
 367 work of Mary Dahl and Maxwell Shepherd for
 368 help preparing documentation.

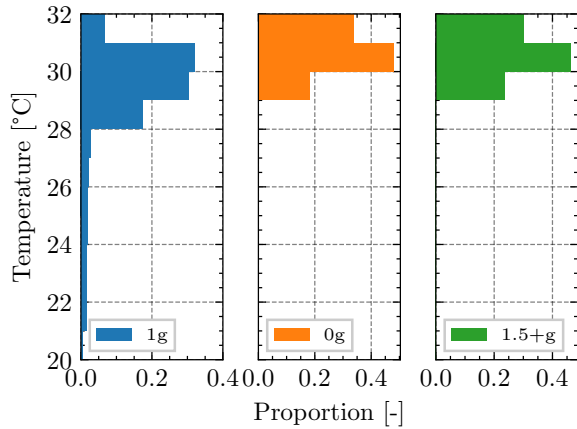


Fig 22: Histogram of temperatures for samples of Corning Varioptic lenses in all gravity conditions, showing that the majority of samples across all regimes are in the 29 °C to 30 °C range.

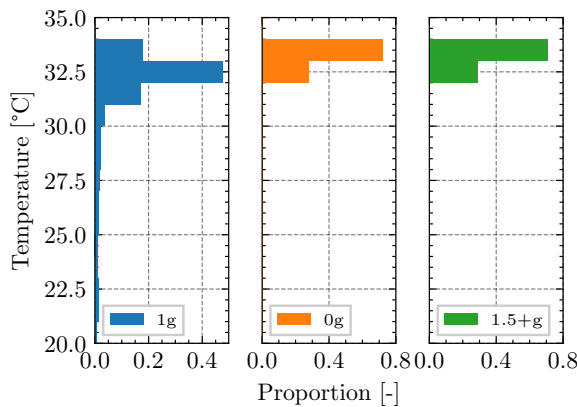


Fig 23: Histogram of temperatures for samples of Optotune lenses in all gravity conditions, showing that the majority of samples across all regimes are in the 32 °C to 34 °C range.

References

- 1 F. A. F. A. Fogle, *Liquid lens beam steering and environmental testing for the miniature optical steered antenna for inter-satellite communication*. Thesis, Massachusetts Institute of Technology (2020). Accepted: 2020-09-03T17:45:43Z.
- 2 F. Fogle, O. Cierny, P. d. V. Pereira, *et al.*, “Miniature Optical Steerable Antenna for Intersatellite Communica-

tions Liquid Lens Characterization,” in *2020 IEEE Aerospace Conference*, 1–13 (2020). ISSN: 1095-323X.

- 3 “Optotune EL-16-40-TC manual.”
- 4 S. Kacker, O. Cierny, J. Boyer, *et al.*, “Link analysis for a liquid lens beam steering system, the miniature optical steered antenna for intersatellite communication: MOSAIC,” in *Free-Space Laser Communications XXXIII*, **11678**, 144–163, SPIE (2021).
- 5 S. Kacker, *Optical Performance and Prototyping of a Liquid Lens Laser Communications Transceiver*. Thesis, Massachusetts Institute of Technology (2022). Accepted: 2022-09-26T19:42:18Z.
- 6 M. Zohrabi, R. H. Cormack, and J. T. Gopinath, “Wide-angle nonmechanical beam steering using liquid lenses,” *Optics Express* **24**, 23798–23809 (2016). Publisher: Optical Society of America.
- 7 “Corning Varioptic Lens Brochure.”
- 8 J. Schneider, “The First Smartphone to Use a Liquid Lens is the Xiaomi Mi Mix Fold,” (2021).
- 9 C. Efstathiou and V. M. Draviam, “Electrically tunable lenses – eliminating mechanical axial movements during high-speed 3D live imaging,” *Journal of Cell Science* **134**, jcs258650 (2021).
- 10 V. Mai and H. Kim, “Variable Focus Lens-Based Beam Steering and Divergence Control for WDM Free-Space Optical Communication,” in *Optical Fiber Communication Conference (OFC) 2022 (2022)*, paper M1C.6, M1C.6, Optica Publishing Group (2022).
- 11 V. Mai and H. Kim, “Optical Beam Control Based on Variable Focus Lenses for WDM FSO Communications,” in *2022 Conference on Lasers and Electro-Optics (CLEO)*, 1–2 (2022). ISSN: 2160-8989.

422 12 S. A. Reza and N. A. Riza, “A liquid lens- 463
423 based broadband variable fiber optical at- 464
424 tenuator,” *Optics Communications* **282**, 465
425 1298–1303 (2009). 466
426 13 N. A. Riza and P. J. Marraccini, “Power 467
427 smart in-door optical wireless link appli- 468
428 cations,” in *2012 8th International Wire- 469
429 less Communications and Mobile Com- 470
430 puting Conference (IWCMC)*, 327–332 471
431 (2012). ISSN: 2376-6506. 472
432 14 N. A. Riza, “Smart Optical Beamform- 473
433 ing for Next Generation Wireless Em- 474
434 powered Communications, Power Trans- 475
435 fer, Sensing and Displays: Building on 476
436 the Past,” in *2022 33rd Irish Signals and 477
437 Systems Conference (ISSC)*, 1–7 (2022). 478
438 ISSN: 2688-1454. 479
439 15 V. V. Mai and H. Kim, “Non-Mechanical 480
440 Beam Steering and Adaptive Beam Con- 481
441 trol Using Variable Focus Lenses for 482
442 Free-Space Optical Communications,” 483
443 *Journal of Lightwave Technology* **39**, 484
444 7600–7608 (2021). Conference Name: 485
445 Journal of Lightwave Technology. 486
446 16 R. W. Gerchberg and W. O. Saxton, “A 487
447 Practical Algorithm for the Determina- 488
448 tion of Phase from Image and Diffraction 489
449 Plane Pictures,” *Optik* **35**, 6 (1972). 490
450 17 D. L. Misell, “A method for the solu- 491
451 tion of the phase problem in electron mi- 492
452 croscopy,” *Journal of Physics D: Applied 493
453 Physics* **6**, L6–L9 (1973). 494

454 **Shreeyam Kacker** is a graduate student in the 496
455 MIT Space Telecommunications, Astronomy, 497
456 and Radiation Laboratory led by Prof. Kerri 498
457 Cahoy. He received the SM degree from MIT 499
458 in Aeronautics and Astronautics in 2022, and 500
459 the MEng degree in Aeronautical Engineering 501
460 from Imperial College London in 2020. His re- 502
461 search specializes in laser communications and 503
462 machine learning applied to remote sensing. 504

List of Figures

- 1 Diagram showing electrowetting principle of operation for Corning Varioptic lenses.⁷
- 2 Diagram showing pressure based principle of operation for Optotune lenses.³
- 3 Block diagram of experiment components.
- 4 Diagram of single optical train in experimental setup.
- 5 Flowchart of experiment flight software that runs continuously and records samples.
- 6 Experimental setup affixed to the floor of the zero gravity aircraft.
- 7 Complete parabolic flight profile of g-force against time showing takeoff, landing, and full 20 parabolas.
- 8 Zoomed view of g-force magnitude over time for second set of five parabolas. All parabolas in this set are zero gravity parabolas.
- 9 Histogram of total samples with g-force of each sample.
- 10 Normalized images of focused individual Corning Varioptic samples from each gravity regime. Increasing gravity shows minor increases in tip/tilt and coma.
- 11 Normalized images of focused individual Optotune samples from each gravity regime. Increases in gravity show larger increases in tip/tilt, coma, and smearing as compared to Fig. 10.
- 12 Relative spot width for sweep of lens commands for Corning Varioptic lenses, with associated hyperbolic fit and error bars.

507 13 Relative spot width for sweep
508 of lens commands for Optotune
509 lenses, with associated hyper-
510 bolic fit and error bars.
511 14 Example Corning Varioptic sam-
512 ple at 53.5 V lens voltage with
513 high relative spot width caused
514 by smeared features.
515 15 Example Corning Varioptic sam-
516 ple with low relative spot width,
517 with identical lens command
518 and gravity conditions as Fig. 14
519 16 Image of stacked and averaged
520 spots for each gravity environ-
521 ment for Corning Varioptic lenses
522 (n: 0 g = 20, 1 g = 206, 1.5+ g
523 = 37).
524 17 Image of stacked and averaged
525 spots for each gravity environ-
526 ment for Optotune lenses (n: 0
527 g = 17, 1 g = 164, 1.5+ g = 26).
528 18 Linear regression of tip/tilt of
529 focused samples against sam-
530 ple gravity conditions.
531 19 Linear regression of tip/tilt of
532 focused samples against sam-
533 ple gravity conditions.
534 20 Potential physical mechanism
535 explaining observed aberrations.
536 Optical fluid sags to the bot-
537 tom of the enclosure, causing
538 slants in the side, which causes
539 tip/tilt like a prism. Addition-
540 ally, fluid curvature on the op-
541 tical membrane creates higher
542 order aberrations, such as coma
543 and astigmatism.
544 21 Temperature profile recorded
545 on Raspberry Pi hat through-
546 out flight. Optotune lenses due
547 to their self heating have a higher
548 temperature throughout the flight.
549 Additionally, each parabola can
550 be seen to have a very small im-
551 pact on recorded temperature.

552 22 Histogram of temperatures for
553 samples of Corning Varioptic
554 lenses in all gravity conditions,
555 showing that the majority of
556 samples across all regimes are
557 in the 29 °C to 30 °C range.
558 23 Histogram of temperatures for
559 samples of Optotune lenses in
560 all gravity conditions, showing
561 that the majority of samples
562 across all regimes are in the
563 32 °C to 34 °C range.

564 List of Tables

565 1 List of hardware used in exper-
566 iment.
567 2 Change in tip/tilt of centroided
568 spots for each regime, refer-
569 enced to 0 g as a baseline.
570 3 Summary of changes in quanti-
571 tatively determined properties
572 of lenses, referenced to 0 g as
573 a baseline.